Fatigue Assessment of Ti–6Al–4V Circular Notched Specimens Produced by Selective Laser Melting

Seyed-Mohammad-Javad Razavi [1], Paolo Ferro [2] and Filippo Berto [1,*]

[1]   Department of Mechanical and Industrial Engineering, Norwegian University of Science and Technology (NTNU), Richard Birkelands vei 2b, 7491 Trondheim, Norway; javad.razavi@ntnu.no

[2]   Department of Engineering and Management, University of Padova, Stradella San Nicola 3, 36100 Vicenza, Italy; ferro@gest.unipd.it

*   Correspondence: filippo.berto@ntnu.no; Tel.: +47-73-59-4129

Abstract: Additive manufacturing (AM) offers the potential to economically produce customized components with complex geometries in a shorter design-to-manufacture cycle. However, the basic understanding of the fatigue behavior of these materials must be substantially improved at all scale levels before the unique features of this rapidly developing technology can be used in critical load bearing applications. This work aims to assess the fatigue strength of Ti–6Al–4V smooth and circular notched samples produced by selective laser melting (SLM). Scanning Electron Microscopy (SEM) was used to investigate the fracture surface of the broken samples in order to identify crack initiation points and fracture mechanisms. Despite the observed fatigue strength reduction induced by circular notched specimens compared to smooth specimens, notched samples showed a very low notch sensitivity attributed both to hexagonal crystal lattice characteristics of tempered alpha prime grains and to surface defects induced by the SLM process itself.

1. Introduction

Additive manufacturing (AM) is a process that allows a part to be built layer-by-layer by using a combination of energy delivery and material deposition. Metallic parts are obtained starting from powders that are melted by a laser or electron beam source. This results in a high sensitivity of material properties to process parameters. According to source parameters, the material can experience different thermal histories and thus different microstructures [1–4]. The microstructure of AM parts can be highly anisotropic and can reach a density greater than 99.5% [5,6]. For example, columnar grains are shown to grow epitaxially through the deposition layers due to cooling [5].

Compared to traditional shaping processes, AM offers different advantages such as a shorter time-to market, a near-net-shape fabrication without the need of expensive molds and tools, a high efficiency in material utilization, the possibility to directly produce geometries with a high level of flexibility based on CAD models. On the other hand, AM parts suffer the presence of defects often related to non-optimal scan parameters (unmolten particles, spherical entrapped gas bubbles, lack of fusion) [7]. Among the AM processes, particular attention is paid to selective laser melting (SLM), a Powder Bed Fusion-Laser (PBF-L) method [8,9]. The possibility to create structures with complex geometries out of high performance materials has made SLM particularly interesting for aerospace and biomedical industries, where titanium alloys—in particular Ti–6Al–4V—are widely used. Titanium alloys are in fact characterized by excellent corrosion resistance, high specific strength, low density, and low elastic modulus.

Both in aerospace and biomedical applications, fatigue is the primary mechanism of rupture in components such as turbine blades, hip prostheses, and mechanical heart valves [10–12]. For this reason, the fatigue strength of additive manufactured parts is widely studied in literature. In their work about High Cycle Fatigue (HCF) behavior of SLM-processed Ti–6Al–4V, Leuders et al. [13] found that porosity acts as a strong stress raiser and leads to failure. In order to improve the fatigue strength of titanium alloy Ti–6Al–4V manufactured by SLM, reduction of porosity was thus considered much more important by authors than microstructure optimization. In a more recent work [14], Kasperovich and Hausmann found a reduction in fatigue resistance of SLM processed TiAl6V4 compared to wrought alloy due to a combination of the unfavorable martensitic microstructure, unmolten particles, pores, and microcracks. Finally, they found that in order to restore the fatigue resistance of the conventionally processed TiAl6V4, SLM-processed samples need to be subjected to Hot Isostatic Pressing (HIP), which reduces porosity and surface machining which reduces surface roughness. As a matter of fact, for AM parts that cannot be machined on all surfaces, the rough 'as built' surface should be considered as a crack initiator in the fatigue design process, leading to their lower fatigue strength. Finally, in that work, heat treatments were found not to provide a significant improvement to HCF strength.

Due to some specific design requirements, such as connecting different parts together and repairing cracked or damaged structures, the majority of engineering components and structures contain notches of different shapes. By their utility, notches are prone to crack nucleation due to the intensified stress in their neighborhood. Nucleated crack(s) may propagate and lead to final failure of the notched component. Hence, it is commonly attempted in design of notched components to prevent or delay the crack nucleation from the notch edge [15–19]. For this aim, failure mechanisms in the presence of notches should be deeply studied.

Examination of the state-of-the-art shows that fatigue assessment and quality assurance of additively manufactured components cannot be performed accurately due to a lack of bespoke methodologies allowing specific microstructural features as well as specific mechanical/cracking behavior of additively manufactured materials to be modelled effectively. Therefore, owing to the growing importance of additive manufacturing technologies, fundamental theoretical understanding of fatigue properties and behavior of additively manufactured metals is a necessary step that must be taken as a matter of urgency. In this challenging scenario, the problem is complicated by the fact that, as far as components having complex geometries are concerned, no specific design criteria have been proposed so far to take into account stress concentration phenomena arising from geometrical discontinuities/features (here termed notches). Furthermore, no fatigue data generated by testing additively manufactured notched metals can be found in the technical literature. This lack of specific knowledge makes it difficult for industry to take full advantage of the unique features of additive manufacturing, preventing this powerful technology from being injected effectively into every-day manufacturing practices. In this context, this work aims to contribute to the fundamental understanding of the mechanical/cracking behavior of additively manufactured Ti–6Al–4V specimens weakened by circular notches and subject to fatigue loading.

2. Material, Geometries, and Experimental Procedure

The analyzed Ti–6Al–4V samples were produced by means of SLM by using optimized process parameters that guaranteed a density greater than 99.7%. Scholars presented various methods of surface treatment for AM components. Conventional surface preparation methods such as machining, mechanical polishing, abrasive flow polishing, chemical milling, and electroplating have been considered for treating the surface of AM components [20–25]. After samples production, specimens were sandblasted at 6 bar using corundum sand with a mean grain size of 220 μm. They were then stress relief heat-treated in non-controlled atmosphere (heating rate: 10.8 °C/min; holding time: 3 h at 650 °C; cooling rate: 2 °C/min) and after cutting off the base plate they were re-sandblasted at 6 bar using corundum sand. All specimens were obtained by using a layer thickness of 60 μm. Figure 1

shows the geometries of smooth and circular notched specimens. The radius at the notch is 5 mm while the thickness of the samples is 3 mm.
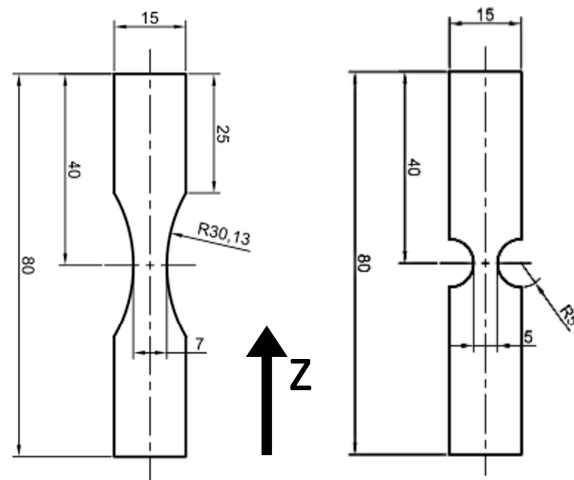

Figure 1. Geometries of smooth and circular notched specimens and built axis (Z) (dimensions in mm).

Fatigue tests were carried out by using a universal MTS machine (250 kN). All tests have been carried out under load control, using a sinusoidal signal in uniaxial tension with a frequency of 10 Hz and load ratio $R = 0$. The run out limit was set to 10^6 cycles. Two specimens were tested for each case of fatigue loading. The microstructure and the fracture surface of the samples were investigated by Optical Microscope and Environmental Scanning Electron Microscope (ESEM), respectively.

Kroll's Reagent (2 mL HF, 2 mL HNO_3, 100 mL H_2O) was used as metallographic etchant. The alpha prime and acicular alpha structures of titanium alloy will appear white after etching while intergranular beta structure and beta grains will be darkened.

A numerical model under plain stress condition was carried out using a commercial numerical code in order to calculate the stress concentration factor, K_t. Young's modulus and Poisson's coefficient were set equal to 110 GPa and 0.34, respectively. By taking advantage of the double symmetry, only one-fourth of the specimen was modelled by using a mapped mesh (Figure 2a). Figure 2b shows the principal stress distribution in the notched specimen.
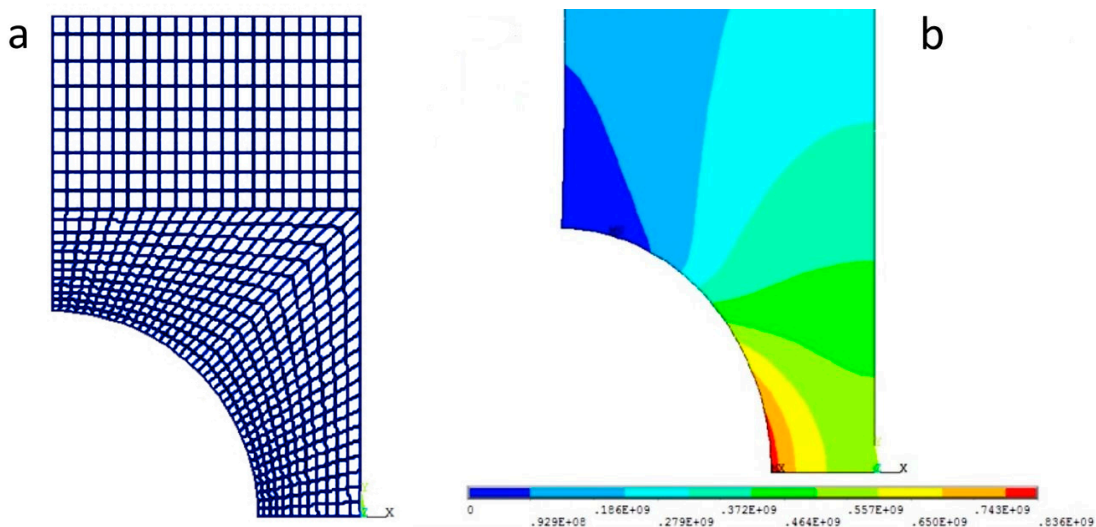

Figure 2. Mesh of the specimen with a double circular notch (**a**) and principal stress (S1) distribution (**b**).

3. Results

3.1. Fatigue Test Results

Results obtained from the statistical elaboration of fatigue test data for smooth and notched samples are reported in Figures 3 and 4, respectively. Values of stress amplitude related to a survival probability of 50%, the slope of the Wöhler curve, and the scatter index T_σ, which is the ratio between the stress amplitudes corresponding to 10% and 90% of survival probability, are reported in the above-cited figures. Specimens that survived over 1 million cycles are considered as run out and marked up with an arrow. It can be noted that the difference between the Wöhler curves are related only to the mean value of the stress amplitude at 1×10^6 cycles, but not to the scatter index T_σ. The fatigue strength of double circular notched specimens at 1 million cycles was 213 MPa compared to a value of 243 MPa related to the fatigue strength of smooth samples.
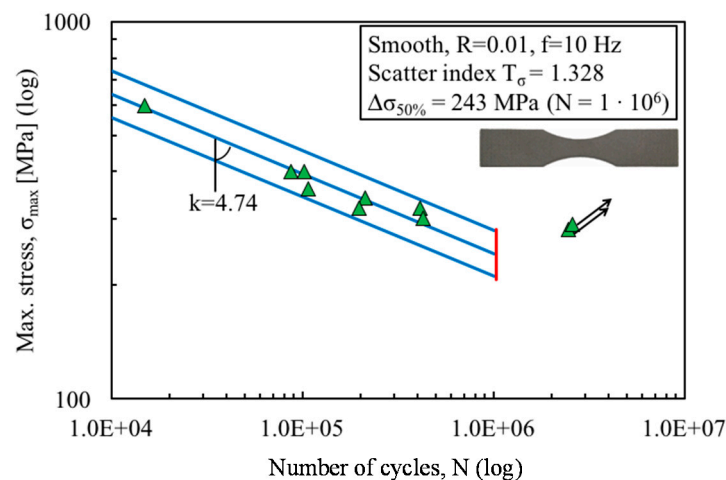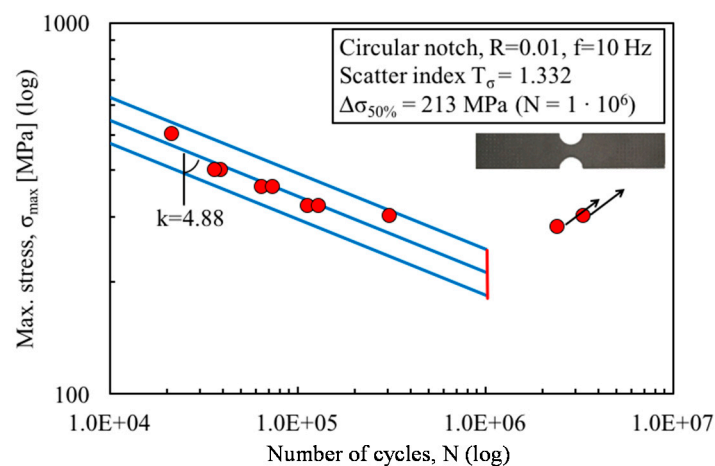

Figure 3. Fatigue life of smooth samples.

Figure 4. Fatigue life of double blunt V-notched samples.

3.2. Microstructure and Fractography

A preliminary microstructure investigation by means of OM showed an almost porosity-free material. Some occasional porosity was found which dimension was less than 50 μm. OM and ESEM micrographs are shown in Figure 5. The grains appear acicular with a prevalence of α′ plates surrounded by a little percentage of β phase. In Figure 5a, the primary equiassic morphology of β phase prior to the β → α′ transformation can be also observed. In Figure 5b, the Al-reach black

zones correspond to α′ phase, tempered by stress-relief heat treatment, while the white zones, reach in vanadium, correspond to β phase. Such a microstructure is due to the high cooling rate that characterizes the SLM process and the subsequent heat treatment below 800 °C.
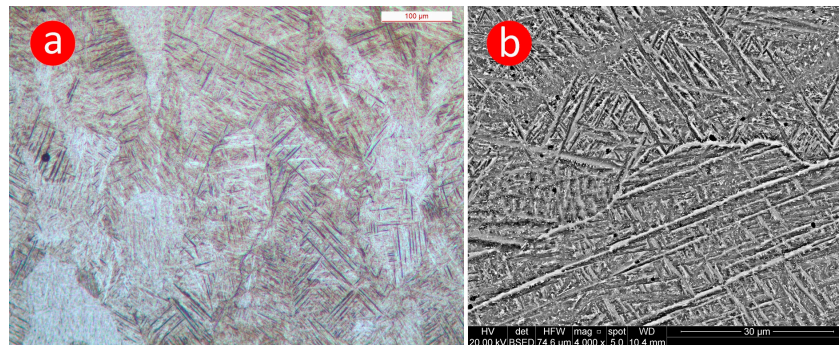

Figure 5. Optical Microscope (**a**) and Environmental Scanning Electron Microscope (**b**) micrographs of the analyzed material.

ESEM fractographs of the smooth and blunt circular notched specimens are shown in Figures 6 and 7, respectively. It is noted that fatigue cracks nucleate at the specimen surface both in smooth and double V-notched specimens where severe intrusions (see Figure 6d), due to the roughness induced by the process, act as crack initiation points (Figures 6d and 7). The fracture nucleates at one point at the surface of the smooth sample (Figure 6d) and propagates towards the opposite edge covering almost the entire cross section of the sample until the final rupture. The final fracture surface, characterized by dimples (Figure 6c), was found to be inclined by about 45° with respect to the load direction (Figure 6a). No porosity was observed on fracture surface of all samples. In a similar way, fatigue cracks nucleate at both notch tips of the double circular notched sample. Thus, the final fracture surface appears in between the two propagation zones and still inclined by about 45° with respect to the load direction. Figure 7 shows a typical deep intrusion where a crack nucleated.
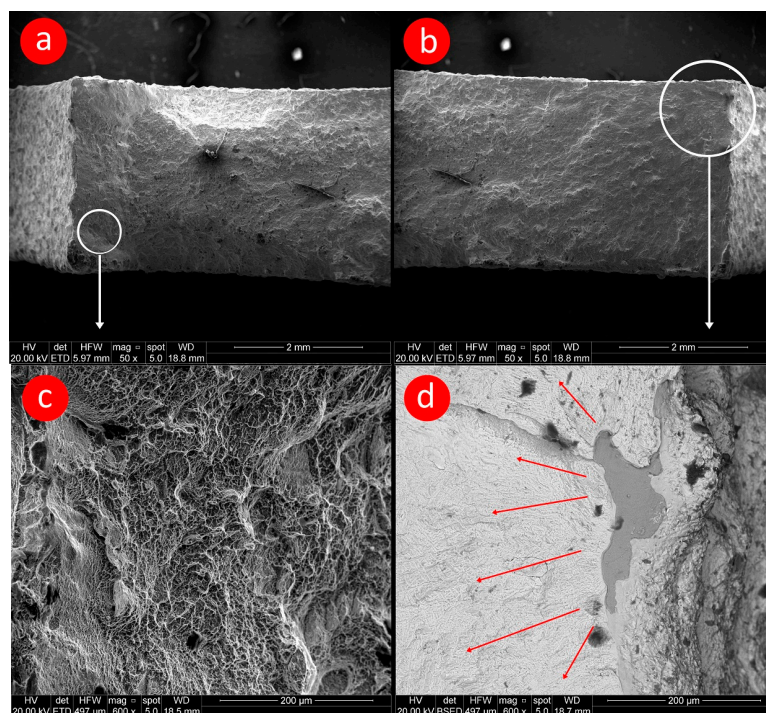

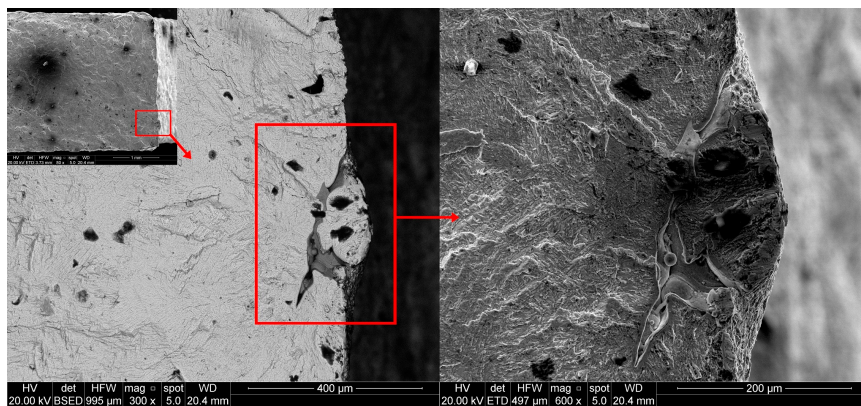**Figure 6.** (**a**–**d**) ESEM fractographs of the smooth specimen (Δσ = 360 MPa, Cycles Number = 106374).

Figure 7. ESEM fractographs of the double circular notched specimen (Δσ = 360 MPa, Cycles Number = 64427).

Finally, despite the several detected high intrusions at the surface that act as easy crack nucleation zones, it was found that fatigue cycles spent for crack nucleation were much higher than those spent for crack propagation (Figure 8).
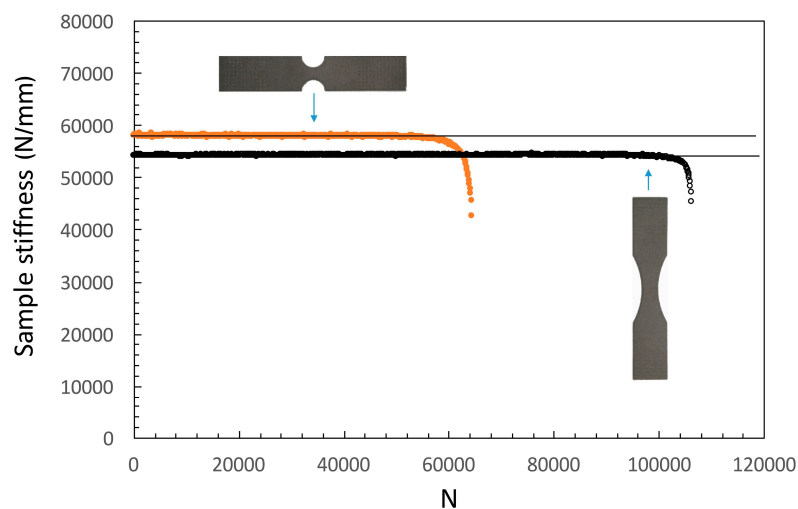

Figure 8. Sample stiffness as a function of cycle number from a smooth and a circular notched sample, both loaded with a nominal stress (σ_n) value of 360 MPa.

In Figure 8, the stiffness of both a smooth and a circular notched sample loaded with the same nominal applied stress (σ_n = 360 MPa) was plotted against the cycles number. It is noted that the stiffness of both samples remains constant for about 90% of the fatigue life. In particular, the crack nucleation period was set equal to the number of cycles beyond which all the experimental points fall down under the interpolation straight line shown in Figure 8. By analyzing all samples with this procedure, it was found that the percentages of fatigue life spent for crack nucleation were 93% and 81% for the smooth and circular notched specimens, respectively.

4. Discussion

By using the obtained experimental data, the notch sensitivity has been calculated. The notch sensitivity (q) is defined by Equation (1):

$$q = \frac{K_f - 1}{K_t - 1} \tag{1}$$

where K_f is the fatigue notch factor ($K_f = \Delta\sigma_A^{smooth}/\Delta\sigma_A^{V-nothc}$) and K_t is the stress concentration factor defined by maximum local stress to nominal stress ratio ($K_t = \sigma_{\max}/\sigma_{nom}$) [26]. The nominal stress is defined as the mean stress across the reduced cross-section of the specimen in the presence of the notch. In general, $0 \leq q \leq 1$. When the theoretical stress concentration factor equals the fatigue notch factor (i.e., $K_f = K_t$), $q = 1$. If the notch has no adverse effect on the fatigue limit (i.e., $K_f = 1$), $q = 0$. By using the fatigue data obtained in this work, $K_f = 1.141$. K_t was found equal to 3.925 by a numerical simulation. This results in a q value equal to 0.048.

A low notch sensitivity of the wrought Ti–6Al–4V alloy was already observed by Hosseini [26]. She justified such alloy behavior through alpha Hexagonal Close Packed (HCP) crystal lattice characteristics. Compared to cubic lattices, such as Face Central Cubic (FCC) or Body Central Cubic (BCC) lattice, the slip planes in HCP lattice are all parallel to each other (planes (0001) in Miller-Bravais system). The slip systems number for dislocations in a HCP lattice are thus very low if compared to those in a Cubic Crystal (CC). Now, dislocations play a key role in the fatigue crack nucleation phase. It has been revealed that after a large number of fatigue loading cycles, dislocations pile up and form structures called Persistent Slip Bands (PSB). Such PSBs can be formed more easily in a crystal grain that has an unfavorable orientation of its slip planes relative to the planes of maximum applied shear stresses (Figure 9). Because of its few slip systems, for a HCP lattice, such unfavorable orientations are very few. In this situation, many potential damage initiation sites occur within the volume of a smooth specimen but, at the sharp notch, it is possible that almost no damage initiation site occurs in the small region around the notch tip where the stress is near its peak value. Hence, considering the local notch stress, the notched member can be more resistant to fatigue.
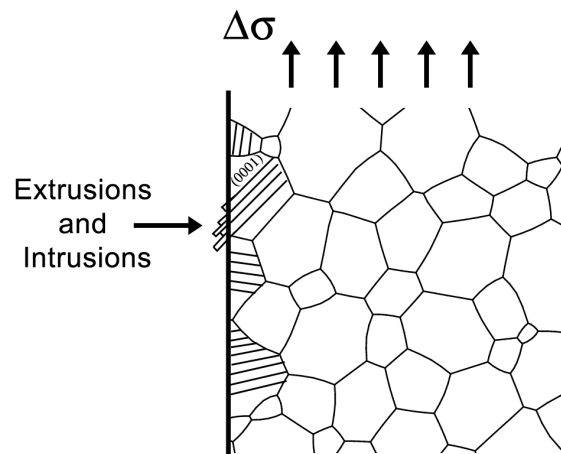

Figure 9. Schematic representation of PSB formed in a crystal grain that has an unfavorable orientation of its (0001) slip planes relative to the planes of maximum applied shear stresses.

In order to better understand the mechanism of crack nucleation in alpha phase, the fatigue test of a specimen with a double circular notch was interrupted when its stiffness values started to fall down. The resulting fatigue cracks were then observed by means of Electron Backscattered Diffraction (EBSD) technique. Figure 10 shows SEM and EBSD micrographs of a fatigue crack and corresponding alpha grain orientation at the initiation and propagation zones. It is observed how the basal slip planes of the alpha grain at the crack initiation zone are oriented about 45° compared to the load direction.

As shown in Figures 6 and 7, fatigue cracks were observed to initiate on severe surface intrusions due to the high roughness induced by the process itself. Such intrusions are covered by an oxide layer which was formed during the stress-relief heat treatment and not cleaned up by the grinding treatment. Now, the number of potential crack initiation intrusions is thought to be much higher in smooth samples than in the sharp V-notch specimen where there is the possibility that no such critical surface defects occur in the small region near the notch tip. It is thought that this effect and the alpha

prime HCP lattice characteristics may justify the very low notch sensitivity of the SLM-processed Ti–6Al–4V alloy observed by experiments. In fact, the surface roughness and imperfections will lead to local surface stress concentrations which make the material exhibit reduced notch sensitivity with respect to notches of higher orders of magnitude than roughness.
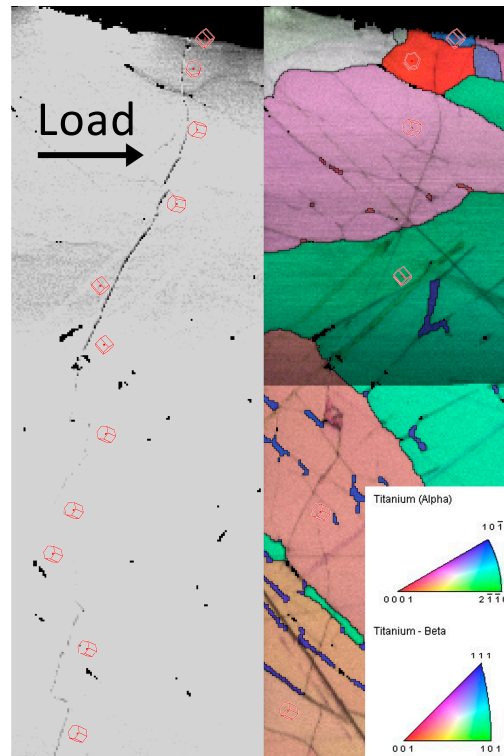

Figure 10. SEM and EBSD micrograph of a fatigue crack in a circular notched specimen.

5. Conclusions

The fatigue strength of Ti–6Al–4V circular notched samples produced by SLM was assessed.

- Results were compared with those corresponding to smooth samples and Scanning Electron Microscopy was used to investigate the fracture surface of broken samples in order to identify crack initiation points and fracture mechanisms.
- Despite the surface treatment and heat treatment of the AM samples, some defects due to manufacturing process were observed on the fracture surface of the tested samples.
- Despite the fatigue specimens being weakened by the sharp circular notch, a very low notch sensitivity was measured.
- Low notch sensitivity of the tested specimens was attributed both to the hexagonal crystal lattice of tempered alpha prime grains and to the high roughness detected on sample surfaces.

Author Contributions: Filippo Berto managed the tests and wrote partially the text, Javad Razavi made the numerical and analytical calculations, Paolo Ferro wrote the text and performed the metallurgical analyses.

Conflicts of Interest: The authors declare no conflict of interest.

References

1. Todai, M.; Nakano, T.; Liu, T.; Yasuda, H.Y.; Hagihara, K.; Cho, K.; Ueda, M.; Takeyama, M. Effect of building direction on the microstructure and tensile properties of Ti–48Al–2Cr–2Nb alloy additively manufactured by electron beam melting. *Addit. Manuf.* **2017**, *13*, 61–70. [CrossRef]
2. Domashenkov, A.; Plotnikova, A.; Movchan, I.; Bertrand, P.; Peillon, N.; Desplanques, B.; Saunier, S.; Desrayaud, C. Microstructure and physical properties of a Ni/Fe-based superalloy processed by Selective Laser Melting. *Addit. Manuf.* **2017**, *15*, 66–77. [CrossRef]
3. Lee, Y.S.; Zhang, W. Modeling of heat transfer, fluid flow and solidification microstructure of nickel-base superalloy fabricated by laser powder bed fusion. *Addit. Manuf.* **2016**, *12*, 178–188. [CrossRef]
4. Lindgren, L.E.; Lundbäck, A.; Fisk, M.; Pederson, R.; Andersson, J. Simulation of additive manufacturing using coupled constitutive and microstructure models. *Addit. Manuf.* **2016**, *12*, 144–158. [CrossRef]
5. Wu, X.; Liang, J.; Mei, J.; Mitchell, C.; Goodwin, P.S.; Voice, W. Microstructures of laser-deposited Ti–6Al–4V. *Mater. Des.* **2014**, *25*, 137–144. [CrossRef]
6. Wycisk, E.; Siddique, S.; Herzog, D.; Walther, F.; Emmelmann, C. Fatigue performance of laser additive manufactured Ti–6A–4V in very high cycle fatigue regime up to 109 cycles. *Front. Mater.* **2015**, *2*. [CrossRef]
7. Vilaro, T.; Colin, C.; Bartout, J.D. As-fabricated and heat-treated microstructures of the Ti–6Al–4V alloy processed by selective laser melting. *Metall. Mater. Trans.* **2011**, *42A*, 3190–3199. [CrossRef]
8. Kruth, J.P.; Mercelis, P.; Van Vaerenbergh, J.; Froyen, L.; Romboust, M. Binding mechanism in selective laser sintering and selective laser melting. *Rapid Prototyp. J.* **2005**, *11*, 26–36. [CrossRef]
9. Vrancken, B.; Thijs, L.; Kruth, J.P.; Humbeeck, J.V. Heat treatment of T6Al4V produced by selective laser melting: Microstructure and mechanical properties. *J. Alloys Compd.* **2012**, *541*, 177–185. [CrossRef]
10. Cherolis, N.E. Fatigue in the Aerospace Industry: Striations. *J. Fail. Anal. Prev.* **2008**, *8*, 255–258. [CrossRef]
11. Song, X.; Wang, L.; Niinomi, M.; Nakai, M.; Liu, Y.; Zhu, M. Microstructure and fatigue behaviors of a biomedical Ti–Nb–Ta–Zr alloy with trace CeO_2 additions. *Mater. Sci. Eng.* **2014**, *619*, 112–118. [CrossRef]
12. Sun, Z.; Chemkhi, M.; Kanoute, P.; Retraint, D. Fatigue properties of a biomedical 316L steel processed by surface mechanical attrition. *Mater. Sci. Eng.* **2014**, *63*. [CrossRef]
13. Leuders, S.; Thöne, M.; Riemer, A.; Niendorf, T.; Tröster, T.; Richard, H.A.; Maier, H.J. On the mechanical behaviour of titanium alloy TiAl6V4 manufactured by selective laser melting: Fatigue resistance and crack growth performance. *Int. J. Fatigue* **2013**, *48*, 300–307. [CrossRef]
14. Kasperovich, G.; Hausmann, J. Improvement of fatigue resistance and ductility of Ti–6Al–4V processed by selective laser melting. *J. Mater. Process. Technol.* **2015**, *220*, 202–214. [CrossRef]
15. Berto, F.; Barati, E. Fracture assessment of U-notches under three point bending by means of local energy density. *Mater. Des.* **2011**, *32*, 822–830. [CrossRef]
16. Berto, F.; Lazzarin, P.; Ayatollahi, M.R. Brittle fracture of sharp and blunt V-notches in isostatic graphite under pure compression loading. *Carbon* **2013**, *63*, 101–116. [CrossRef]
17. Berto, F.; Lazzarin, P.; Marangon, C. Fatigue strength of notched specimens made of 40CrMoV13.9 under multiaxial loading. *Mater. Des.* **2014**, *54*, 57–66. [CrossRef]
18. Razavi, S.M.J.; Ayatollahi, M.R.; Sommitsch, C.; Moser, C. Retardation of fatigue crack growth in high strength steel S690 using a modified stop-hole technique. *Eng. Fract. Mech.* **2017**, *169*, 226–237. [CrossRef]
19. Ayatollahi, M.R.; Razavi, S.M.J.; Sommitsch, C.; Moser, C. Fatigue life extension by crack repair using double stop-hole technique. *Mater. Sci. Forum* **2017**, *879*, 3–8. [CrossRef]
20. Blattmeier, M.; Witt, G.; Wortberg, J.; Eggert, J.; Toepker, J. Influence of surface characteristics on fatigue behaviour of laser sintered plastics. *Rapid Prototyp. J.* **2012**, *18*, 161–171. [CrossRef]
21. Krahmer, D.M.; Polvorosa, R.; de Lacalle, L.N.L.; Alonso-Pinillos, U.; Abate, G.; Riu, F. Alternatives for Specimen Manufacturing in Tensile Testing of Steel Plates. *Exp. Tech.* **2016**. [CrossRef]
22. Vaithilingam, J.; Goodridge, R.D.; Christie, S.D.; Edmondson, S.; Hague, R.J.M. Surface modification of selective laser melted structures using self-assembled monolayers for biomedical applications, Polishing. In Proceedings of the Solid Freeform Fabrication (SFF) Symposium, Austin, TX, USA, 6–8 August 2012.
23. Yadroitsev, I.; Smurov, I. Surface morphology in selective laser melting of metal powders. *Phys. Procedia* **2011**, *12*, 264–270. [CrossRef]

24. Yang, L.; Gu, H.; Lassell, A. Surface treatment of Ti6al4V parts made by powder bed fusion additive manufacturing processes using electropolishing. In Proceedings of the Solid Freeform Fabrication (SFF) Symposium, Austin, TX, USA, 4–6 August 2014.

25. De Lacalle, L.N.L.; Lamikiz, A.; Sanchez, J.A.; Arana, J.L. Improving the surface finish in high speed milling of stamping dies. *J. Mater. Proc. Tech.* **2002**, *123*, 292–302. [CrossRef]

26. Hosseini, S. Fatigue of Ti–6Al–4V. In *Biomedical Engineering—Technical Applications in Medicine*; Hudak, R., Penhaker, M., Majernik, J., Eds.; InTech: Rijeka, Croatia, 2012; ISBN 978-953-51-0733-0.